The structure and the properties of WC-Co samples produced by SLM technology and carbon-doped prior to HIP processing

David Bricín
Department of Material Science and Technology, University of West Bohemia, Pilsen, Czech Republic and Centrum vyzkumu Rez s r o, Pilsen, Czech Republic
Filip Véle
Faculty of Mechanical Engineering, Technical University of Liberec, Liberec, Czech Republic
Zdeněk Jansa
New Technologies Research Centre, University of West Bohemia in Pilsen, Pilsen, Czech Republic
Zbyněk Špirit
Centrum vyzkumu Rez s.r.o., Pilsen, Czech Republic
Jakub Kotous
COMTES FHT a.s., Dobrany, Czech Republic, and
Dana Kubátová
Metrology Laboratory Regional Technological Institute, University of West Bohemia in Pilsen Faculty of Mechanical Engineering, Pilsen, Czech Republic

Abstract

Purpose – The purpose of this study is to verify how the carbon doping of the WC-Co cemented carbide (CC) affected their structure before their processing by hot isostatic pressing (HIP) technology.

Design/methodology/approach – The samples for this experiment were fabricated by selective laser melting technology (SLM) using a YAG fiber laser with a power of P = 40 W and a scanning speed of 83 mm/s. The subsequent carbon doping process was performed in a chamber furnace at 900 0 C for 1, 4 and 12 h. The HIP was performed at 1,390°C and pressures of 40 MPa, 80 MPa and 120 MPa. The changes induced in the structures were evaluated using X-ray diffraction and various microscopic methods.

Findings – X-ray diffraction analysis showed that the structure of the samples after SLM consisted of WC, W_2C, Co_4W_2C and Co phases. As a result of the increase in the carbon content in the structure of the samples, the transition carbide W_2C and structural phase Co_4W_2C decayed. Their decay was manifested by the coarsening of the minor alpha phase (WC), which occurred both during the carburizing process and during the subsequent processing using HIP. In the samples in which the structure was carburized prior to HIP, only the structural phases WC and Co were observed in most cases.

Originality/value – The results confirm that it is possible to increase the homogeneity of the CC structure and thus its applicability in practice by additional carburization of the sample structure with subsequent processing by HIP technology.

Keywords Cemented carbides, WC-Co, SLM process, HIP process, Eta phase

Paper type Research paper

Introduction

Additive technologies, also known as 3D printing, are used in a wide range of applications, including the processing of cemented carbides (CCs) (M, 2020; Uhlmann *et al.*, 2015; Brookes, 2019). CCs are particulate composite materials that usually consist of tungsten carbide hard phase particles (WC) and a metallic tough binder of Co, Fe or Ni surrounding the particles (Upadhyaya, 1998). In addition to these components, they may contain other structural phases that affect their

The current issue and full text archive of this journal is available on Emerald Insight at: **https://www.emerald.com/insight/1355-2546.htm**

Rapid Prototyping Journal
28/11 (2022) 102–122
Emerald Publishing Limited [ISSN 1355-2546]
[DOI 10.1108/RPJ-04-2022-0106]

Received 8 April 2022
Revised 4 August 2022
Accepted 31 August 2022

microstructures and mechanical and physical properties. These phases include, for example, inhibitors of WC grain growth (VC, NbC, TaC), which prevent coarsening during the sintering process or graphite phases or transition carbides of the M_6C group ($Co_{3.2}W_{2.8}C$ – Co_2W_4C) or $M_{12}C$ (Co_6W_6C), which are referred to as eta phases (Morton *et al.*, 2005; Upadhyaya, 1998). η-phases and graphite phases can negatively affect the mechanical properties of CC, and their presence in the CC structure is usually considered undesirable (Eso *et al.*, 2007; (Sun *et al.*, 2011). How these phases affect the mechanical properties of CC is also dependent on how these phases are distributed in the CC volume, their morphology, size and volume fraction (Sun *et al.*, 2011; Formisano *et al.*, 2016). The WC-Co phase diagram (Figure 1) shows the carbon ratios and temperatures at which the eta phase can form and when graphite can form in the CC structure.

In addition to the carbon deficit in Co-rich regions, the rate at which the CC structure cools from the sintering temperature leads to the formation of the η-phase (Upadhyaya, 1998; García *et al.*, 2019). If the cooling rate is gradual, the eta phase decays, which is associated with the coarsening of the major phase of tungsten carbide (Vreeswijk *et al.*, 2021). In the case of high carbon deficiency, the η-phase is retained in the CC structure during both rapid and gradual cooling from the sintering temperature (Upadhyaya, 1998).

In the processing of CC by selective laser melting (SLM), the formation of the η-phase is supported by the evaporation of the material during this process, the volume of which depends on the energy density introduced, as shown in equation (1) (Bai *et al.*, 2019), and the processing strategy of the deposited powder bed (Fortunato *et al.*, 2019).

$$E_{vd} = \frac{P}{v \cdot h \cdot t} \left[\frac{J}{mm^3}\right] \quad (1)$$

where $E_{vd}\left[\frac{J}{mm^3}\right]$ is the bulk energy density; P [W] is the laser power; $v\left[\frac{mm}{s}\right]$ is the laser spot motion velocity; t [mm] is the height of the deposited powder layer; and h [mm] is the spacing between laser spot motion vectors (Bai *et al.*, 2019).

This resulted in the formation of carbon-deficient regions in the CC volume, in which the precipitation of the η-phase was enabled by the conversion of WC grains during solidification (Yang *et al.*, 2020; Kublii and Velikanova, 2004). Its formation depends on the contents of dissolved W and C in the solid solution of Co (Yang *et al.*, 2020; Pollock and Stadelmaier, 1970). Laser energy further influenced the formation of pores and cracks in the CC structure. At high values, the porosity of the material structure is reduced (Fortunato *et al.*, 2019; Kumar, 2009), because of the evaporation of the binder and because the heating of the material is not uniform, large transverse and longitudinal tensile residual stresses are generated, which cause cracking of the CC structure after solidification (Gusarov *et al.*, 2011). The microstructure of CC is composed of fine WC grains in some locations and coarse grains in others (Domashenkov *et al.*, 2016), as shown in Figure 2. This heterogeneous distribution of the tungsten carbide grain size in the CC volume is due to the way the material is processed using SLM. When the laser beam interacts with the powder bed, it melts the deposited powder layers and heats their immediate surroundings (i.e. the previously deposited layers). This then leads to a gradual coarsening of the WC grains in these areas, during which multi-layered growth of WC grains can be observed (Gu and Meiners, 2010). It was observed that coarser WC grains were located along the boundaries of the molten region and finer ones inside it. This is due to the high cooling gradient induced by powder bed processing (Campanelli *et al.*, 2019).

The occurrence of CC structural defects can be limited in various ways. For example, the formation of cracks can be prevented in the CC structure by increasing the binder content (Khmyrov *et al.*, 2016), by multiple remelting of the powder layer (Fortunato *et al.*, 2019) or by preheating the build platform to high temperatures (Fries *et al.*, 2020). The occurrence of pores can be influenced by the type and quality of the powder used (Chen *et al.*, 2019) and its processing parameters (Uhlmann *et al.*, 2015). In addition, various post-processing technologies can be used to improve the quality of printed samples. These include mechanical surface treatment of the material (Portella *et al.*, 2020; Lu and Lu, 2004) and heat treatment (HT) technologies (Nicoletto *et al.*, 2017; Kučerová *et al.*, 2021). During HT, the residual stresses

Figure 1 Phase diagram of WC-Co-C for a system with 10 Wt. % Co (Bricín, 2019)

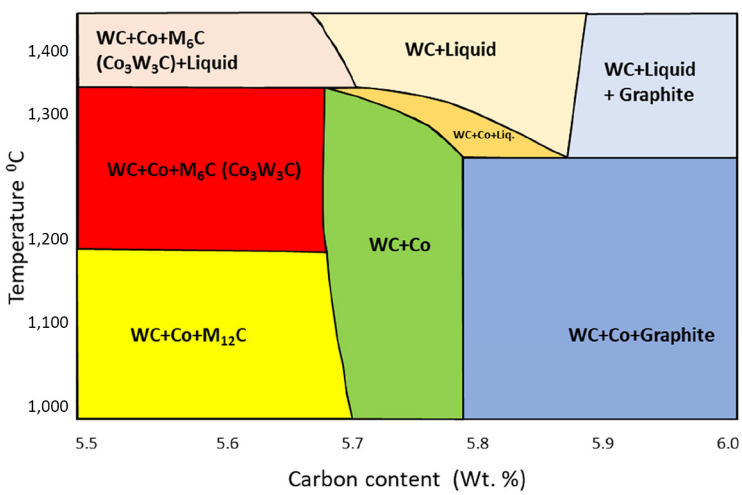

Figure 2 Structure of WC-Co sample after SLM. The structure of WC grains was visualized by chemical etching using Murakami etchant

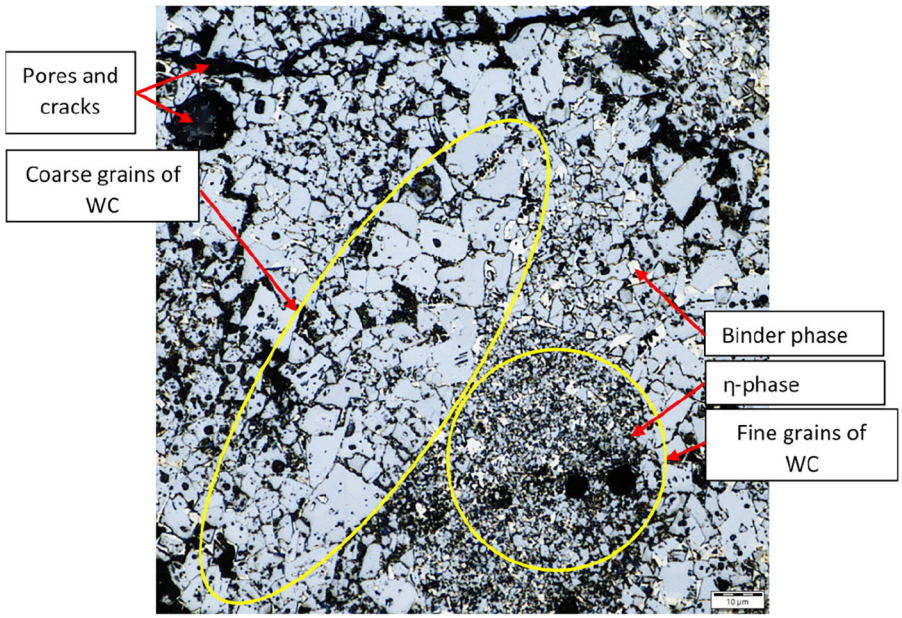

Notes: The light blue-grey areas are formed by WC grains. The white areas are formed by the binder. The dark areas are pores, cracks and η-phases

in the CC structure can be gradually released owing to the increased temperature; thus, its wear resistance can be affected (Stewart *et al.*, 1998). When applying additional pressure using hot isostatic pressing (HIP), we can achieve a reduction in the porosity of the product (Ku *et al.*, 2019). In addition, we can use active atmospheres in HT, which can induce different phase transformations in the product structure, thereby influencing the emerging microstructure of the product (Budin *et al.*, 2017). In this study, we considered the use of a combination of chemical HT with HIP as a finishing technology in the processing of WC-Co samples produced by SLM. In the experiment, some of the samples processed via SLM were subjected to chemical HT. During this process, the proportion of carbon in the structure and binder increased. Subsequently, all the samples were processed by isostatic hot pressing. The differences in the microstructure of the samples caused by their different treatments were then evaluated by X-ray diffraction analysis and metallographic analysis using light, electron and confocal microscopy methods.

Materials and methods

As in a previous study (Bricín *et al.*, 2020), a commercially available WC-Co powder blend, designated AM WC701, was used as the experimental material. This material was supplied by Global Tungsten and Powders s.r.o., Bruntál (CZE). The powder mixture consisted of a granulate with a predominantly spherical powder particle shape (Figure 3). Different types of defects were identified in the powder particles by scanning electron microscope (SEM) analysis, including surface and internal cavities or the interlocking of multiple powder particles, as shown in Figure 3. This can negatively affect the quality of the processed powder layer, thus increasing the porosity of the formed products (Sames *et al.*, 2016). The tungsten carbide grains identified in the powder particles had a triangular shape, which is typical of tungsten carbide, owing to its internal crystalline structure. The initial chemical composition of the powder particles was determined using energy dispersive X ray analysis chemical composition analysis. Measurements were performed using the spot method from the surface of the powder particles. The particles consisted of 21.7 ± 2.6 Wt.% of Co binder, and the remainder consisted of tungsten carbide grains (Table 1).

The supplied material was processed using a SLM 280HL printer (SLM Solutions Group AG, Lübeck, Germany). This printer had a Yb:YAG (IPG Photonics) filament laser with a maximum power of 400 W. For this experiment, the blade-shaped specimens with external dimensions of $17.6 \times 14.7 \times 7.6$ mm [Figure 4(a)] were fabricated on a 280×280 mm platform made of S235 steel. For a reliable connection with the platform, an additional volume of 2 mm thickness was defined on the bottom surface of the specimen, which can be removed after fabrication by conventional machining methods. The thickness of the powder layer was then chosen to be 40 μm. During the processing of the powder bed, the laser vectors were tilted at an angle of 45° to the inert atmosphere flow [Figure 4(b)] and in the following layer, the laser scanning grid was rotated 90° with respect to the previous processed powder layer. Laser power P = 40 W and scanning speed 83 mm/s were used to process the powder bed. The powder bed process was performed under a protective atmosphere of generator nitrogen with a purity of 97%–98%. Using the above parameters (Table 2) results in samples with a relatively high degree of porosity. However, this increases the area through which carbon can diffuse into the CC material. This setting was intended to increase the efficiency of the subsequent carburizing.

Figure 3 (a) Surface structure of the powder particles; (b) section through the powder particle, the distribution of Co binder and WC particles can be observed; and (c) satellite connection between two particles of the powder used

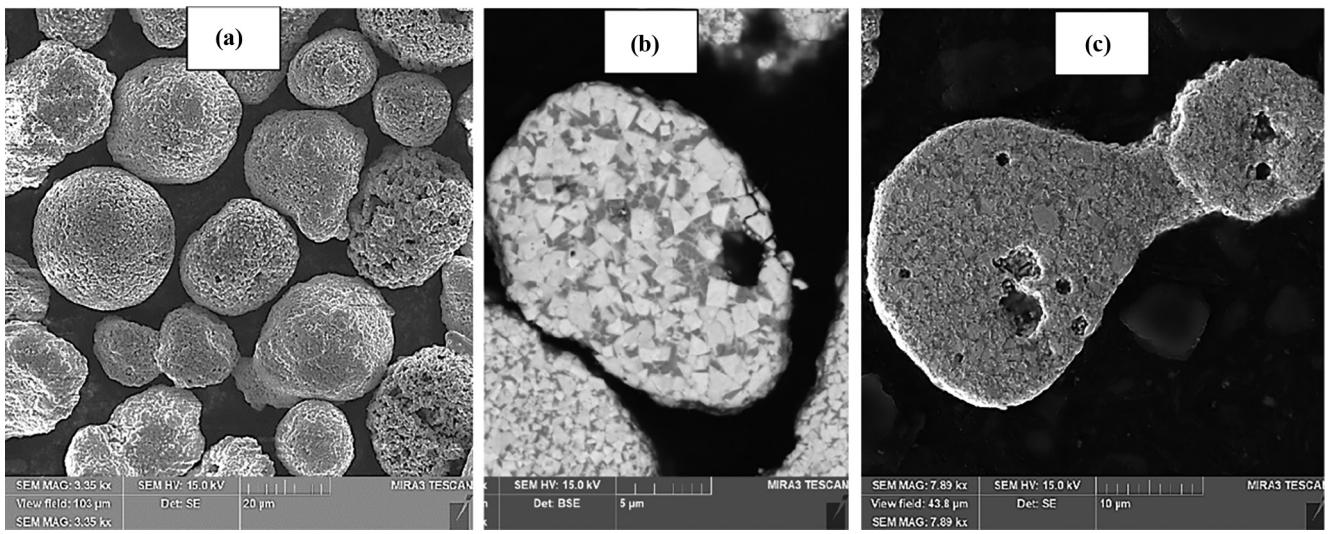

Table 1 AM WC701 material composition table (GTP, 2022)

Chemical composition		Particle size distribution [μm]			Application
WC [%]	Co (%)	D10	D50	D90	Binder Jetting
rest	11–13	10–25	20–30	>30	

Figure 4 (a) Model of the WC-Co wafer for carbon saturation tests; (b) representation of the laser vectors in a single layer, including the direction of flow of the inert atmosphere

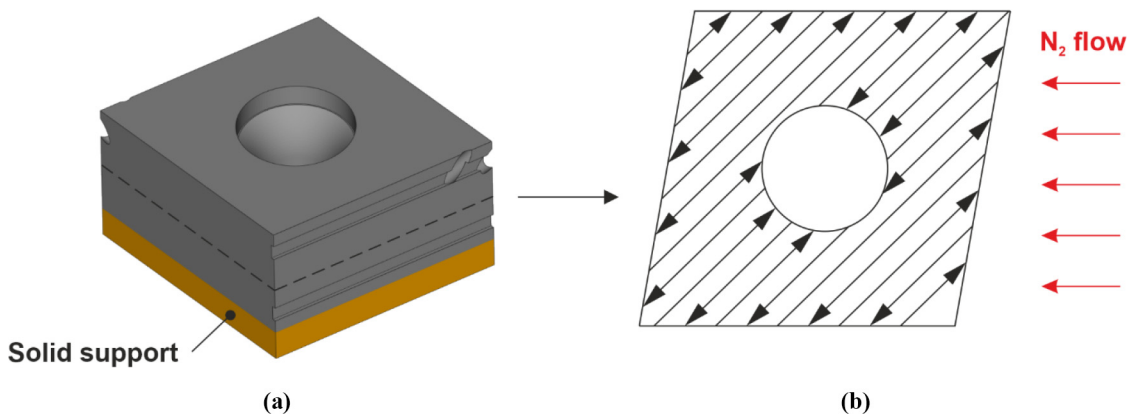

Table 2 SLM process parameters

Power [W]	Speed [mm/s]	Energy density [J/mm^3]	Hatch distance [mm]	Layer thickness [mm]	Atmosphere
40	83	120	0.1	0.04	Nitrogen

The carburizing process was carried out in a granulate backfill with the trade name Durferrit supplied by AZ PROKAL s.r.o. (Brno, CZE). The process was performed in a chamber furnace (LAC s.r.o., Židlochovice, CZE) at 900°C for 1, 4 and 12 h (Table 3).

In the carburizing process, the maximum solubility of carbon in the binder of the processed WC-Co samples depends on the processing temperature. At the selected carburizing temperature of 900°C, the amount of carbon at the interface between the Co phase and the surrounding atmosphere corresponds in the short time to a value of approximately 0.15 Wt.% C (ASM International, 1992). This amount will vary further from this interface depending on how much carbon was dissolved in the binder, Co, prior to the

Table 3 Carbon doping process parameters

Temperature [°C]	Heating rate [°C/s]	Holding time [hours]
900	0.125	1–12

carburizing process and on how much carbon is transferred into the binder from the alpha major phase and the minor phases present. If we consider that during the carburizing process the concentration differences of individual elements are gradually equalized, it is possible to conclude that the proportion of carbon in the binder does not exceed the value of its maximum solubility in this phase. If the maximum solubility of carbon in the solid solution of the binder Co is exceeded, then free carbon or graphite would be excluded. Under certain conditions, the formation of metastable structural phases such as the Co_2C or Co_3C phase could then also occur (Ishida and Nishizawa, 1991). In addition to these phases, the WC phase may be converted to metastable W_2C structure or more complex types of transition carbides (Kumar, 2018). In addition to the above, at high cooling rates from the selected carburizing temperature, a thin layer of free carbon at the interface between the WC grains and the Co binder may be excluded (Ponomarev *et al.*, 2015). During carburization, carbon diffusion occurs in tungsten carbide particles mainly through a vacancy diffusion mechanism (Lassner and Schubert, 2012). The rate of carbon diffusion in tungsten carbide particles is thus slower compared to other structural components. Therefore, it is likely that tungsten carbide particles in contact with the surrounding carburizing atmosphere will develop a layer of free carbon at their interface. At greater distances from this interface, the tungsten carbide particles will then tend to release carbon into the Co binder as mentioned above. Thus, at the interface of these phases, the conditions will be suitable for the formation of the metastable structures and complex types of transition carbides. The formation of the above structural phases is largely dependent on the delay and carburizing temperature and the cooling rate from this temperature. With gradual cooling, the distance the carbon is then able to diffuse can be calculated using the diffusion equations 2–6 below (Ptáček, 2003).

$$\frac{\partial_C}{\partial_\tau} = \frac{\partial}{\partial_x} \cdot \left(D \cdot \frac{\partial_C}{\partial_X} \right) \tag{2}$$

$$erf(z) = \frac{2}{\sqrt{\pi}} \cdot \int_0^Z e^{-t^2} dt = 2 \cdot \ \Phi \cdot \left(x \cdot \sqrt{2} \right) - 1 \tag{3}$$

$$\Phi(u) = \int_{-\infty}^{u} \frac{1}{\sqrt{2 \cdot \pi}} \cdot e^{-\frac{t^2}{2}} dt \tag{4}$$

Where:

D [m^2s^{-1}] is diffusion coefficient; c [Wt.%] is volume concentration of the given element; τ [s] is time during which diffusion occurs; x [m] is position coordinate of the diffusion flow direction; $e_{rf}(z)$ is Gaussian error integral; and $\Phi(u)$is normal distribution function.

For the saturation of a given environment by an element, then the solution of the above equations of the second Fick's law can be obtained by equation (5). By solving it, the concentration gradient in each region can then be determined, see equation (6):

$$\frac{c - c_0}{c_1 - c_0} = 1 - erf\left[\frac{x}{2 \cdot (D \cdot \tau)^{\frac{1}{2}}} \right] \tag{5}$$

$$c = c_1 + \frac{c_2 - c_1}{2} \cdot [1 - \mathrm{erf}(z)] \tag{6}$$

Where:

c [Wt.%] is the calculated concentration value, c_0, c_1, c_2 [Wt.%] are concentration values.

The graph, see Figure 5, then shows the difference in the achieved carburization depths if we consider that the carbon passes from the carburizing atmosphere through a pure cobalt environment.

However, in the printed WC-Co samples, the proportion of binder is relatively small and its free length among tungsten carbide particles corresponds to fractions of units to tens of micrometers. For this reason, and because the structure of the formed samples is composed of a large proportion of interconnected pores which coming up to their surface (so-called open porosity), it can be concluded that the actual depth of carburization in their case was different and nonuniform in various directions. This is also because the structure of the samples is quite heterogeneous after SLM preparation.

The isostatic hot-pressing process was carried out in cooperation with the University of Ostrava (Ostrava, CZE), using a P25004 laboratory unit (Engineered Pressure Systems International nv [EPSI], Temse, Belgium). The processing temperature was set at 1,390°C and the pressures were set at 40 MPa, 80 MPa and 120 MPa. The temperature duration was set to 1 h (Table 4). Subsequently, the samples were cooled by switching the heating elements off. Argon was used as the protective atmosphere.

In isostatic hot pressing, components are exposed to high temperature and external pressure. As a result, their closed porosity is suppressed, and the homogeneity of their structure is increased (Sarin, 2014). One of the reasons why these changes occur is the temperature of the process and the holding time at this temperature. At low temperatures of the sintering process, there is not enough liquid phase to wet the tungsten carbide grains, and so the capillary forces that squeeze these grains together are weak, unable to significantly affect their position, and so there is no significant increase in the density of the products. The magnitude of the capillary forces applied is also affected by the applied pressure. At higher values, similarly to higher sintering temperatures, the density of the products increases significantly (Sarin, 2014). Another factor affecting the final structure of the products is the holding time at sintering temperature and the rate of cooling from this temperature. During the sintering temperature retention, the small carbides gradually dissolve into the molten Co binder and reprecipitate on the coarse grains, resulting in coarsening of the large carbide grains. The dissolution of small WC grains occurs primarily at sites with higher activation energy values, i.e. sites under compression (Sarin, 2014). At high sintering temperatures or a long time at this temperature, significant coarsening of WC grains and in some cases, porosity is formed due to evaporation of structural components of the binder Co. On cooling from the sintering temperature, the solubility of tungsten and carbon in the binder then decreases, leading to the re-precipitation of carbides. Depending on the proportion of components in the Co binder and the rate of cooling, the

Figure 5 Comparison of the carbon concentration gradient in the Co binder at different carburization times and temperature 900°C

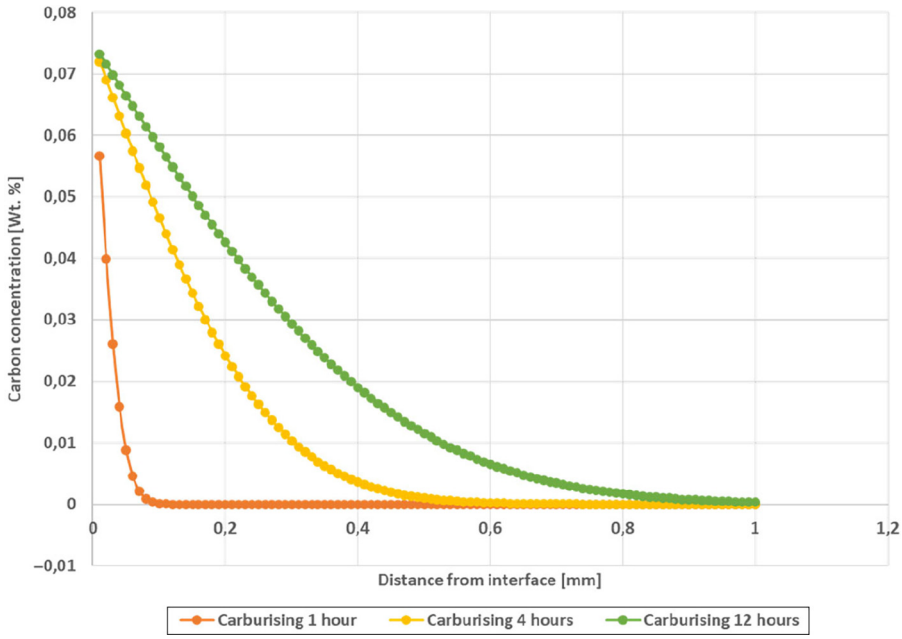

Table 4 HIP process parameters

Temperature [°C]	Heating rate [°C/s]	Holding time [hours]	Pressure [MPa]
1,390	0.154	1	40–120

formation of the eta phase or other types of carbides may then occur (Upadhyaya, 1998).

All samples were subsequently analyzed for changes in the phase composition, crystallite size of the minor WC phase and size of micro deformations using a Panalytical X'Pert PRO automatic X-ray diffractometer (Malvern Panalytical, Eindhoven, The Netherlands). Because of the elements present in the samples, a copper cathode X-ray source with a wavelength of $\lambda K\alpha 1 = 0.15405980$ nm was used. A standard Bragg-Brentano setup with a symmetric geometry was used for the measurements. The samples were measured over angles ranging from 30° to 100° [2ϑ]. A PIXcel1D ultrafast semiconductor detector was used to collect diffracted radiation. All data were evaluated in the same manner to allow full comparison of all samples and to obtain relevant data. The measured data were first processed using the High Score software and subsequently evaluated using the Peak Fit software. Comparison and graphical processing of the measurement results were performed using Origin software.

The surface topography of the samples was evaluated using an Olympus Lext OLS5100 confocal microscope (Olympus Czech Group, s.r.o., Prague, CZE) in a 10× objective configuration with a field of view of 1,281 μm × 1,279 μm. The Olympus Data Acquisition software was used for data acquisition. The Olympus Data Analysis software was used for data analysis. The samples were also subjected to metallographic analysis. The aim was to compare the changes in porosity, distribution, shape and size of the major phases of the WC and Co binder in the bulk samples after different treatments. Scanning electron microscopy (SEM, Philips XL30ESEM, FEI Company, Hillsboro, Oregon, USA) and Tescan Mira3 (TESCAN ORSAY HOLDING, a.s., Brno, CZE) were used for the structural analysis of the samples. The analysis of these microscopes was performed in secondary electron (SE) and Back Scattered Electron (BSE) modes in combination with local analysis of the change in the chemical composition of the samples by energy-dispersive X-ray spectroscopy (EDS). The acquired metallographic images were then analyzed using NIS elements software (Laboratory Imaging s.r.o., Prague, CZE). Murakami etching was used to develop microstructures of the samples. The etching procedure for identifying the structural phases was based on ASTM B657 (ASTM, 2000).

Experimental results and discussion

Metallographic analysis

The first step of the metallographic analysis was a study aimed at evaluating changes in the surface morphology of samples that had been processed using the above methods.

The measurements were made to determine the surface requirements of the samples for their machining for additional shape modifications, e.g. chip formers by laser manufacturing; see ref (Stankevič, 2018). The surface finish demand of the samples is determined by the proportion of protrusions and depressions that form the surface structure of the samples after the SLM process, which in the case of surface evaluation is significantly related to the so-called material support fraction or Abbott curve parameters. It was measured in two perpendicular planes. The first plane was the print plane, the XY plane, the second measurement was made in the XZ plane see Figure 6(a).

To fully evaluate and extract as much information as possible from this test, the measurements were made using both profile and Abbot curve surface roughness assessments. The Abbot

Figure 6 (a) Samples produced in the experiment; (b) elevation profile of the surface structure XZ plane; and (c) elevation profile of the surface structure XY plane (top layer)

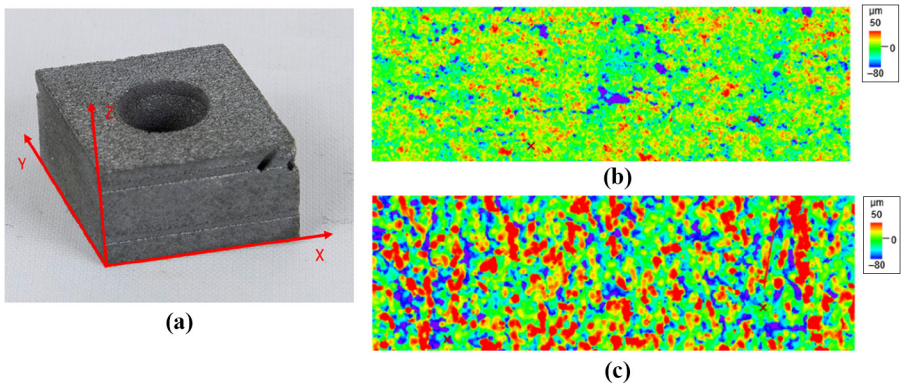

curve was chosen based on the study conducted and described in ref (Kubatova and Melichar, 2019). In the second step, the measurement was performed for the surface roughness (mainly to obtain a visual representation of the surface texture) which can be seen in Figure 6(b)–6(c) to complement the information from the profile measurement. However, for the evaluation of the experiment described above, the main supporting element is precisely the parameters of the Abbott curve summarized below:

- Rv – the greatest depth of the profile depression;
- Rp – the greatest height of the profile protrusion;
- Rvk – reduced groove length; and
- Rpk – reduced height of the tip.

Initially, the parameters Rvk and Rpk were evaluated. The graphs in Figure 7, show the averaged values from five measurements of these parameters, which tell about the change in the size of depressions and protrusions on the surface of the analyzed samples.

From a first comparison of the data in Figure 7, a slight decrease in surface roughness values was observed during HIP processing for all processing methods evaluated. This was already due to imperfections from the production and preparation of the samples where there was a large porosity of the tested parts mainly in the XY direction for which the results are shown in Figure 7. To confirm or refute this claim, only the local maxima and minima were evaluated using the parameters Rv and Rp for both XZ and XY directions; see Figure 8.

From the data presented in Figure 8, it can be seen that for the samples after the HIP process, evaluated at local maxima, there was a clear reduction in the value of both the linear roughness profile Rp and the linear roughness profile Rv. A more pronounced change in their value is then evident in the direction of the print construction, i.e. in the XZ direction evaluated, where, due to the porosity of the initial sample, the surface may have been fused and unified. For the samples that have undergone carburizing before the HIP process, a similar

Figure 7 Comparison of the observed change in the linear roughness profile parameters Rpk and Rvk for samples before and after HIP treatment

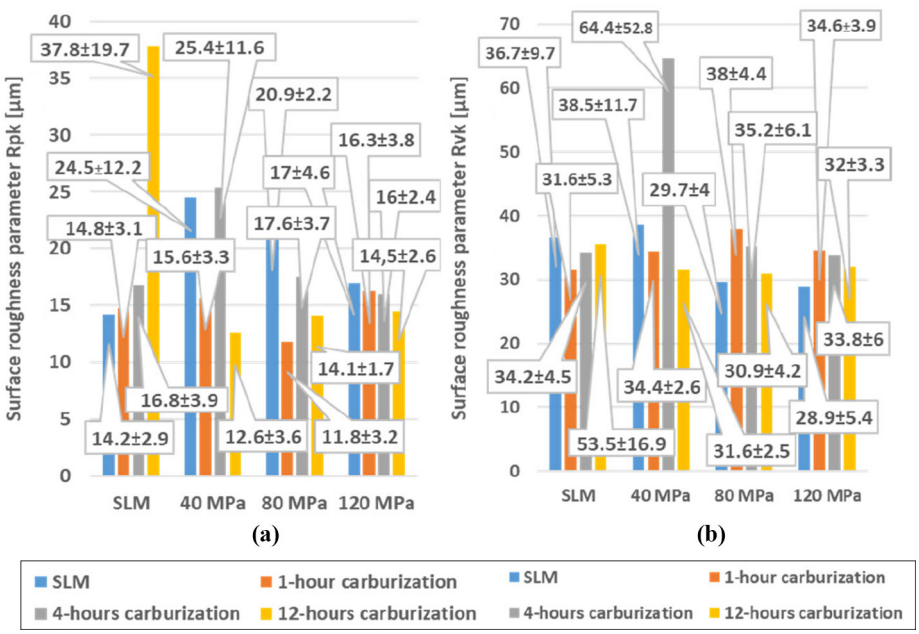

Figure 8 Comparison of the observed change in linear profile roughness parameters Rp and Rv for samples before and after HIP treatment

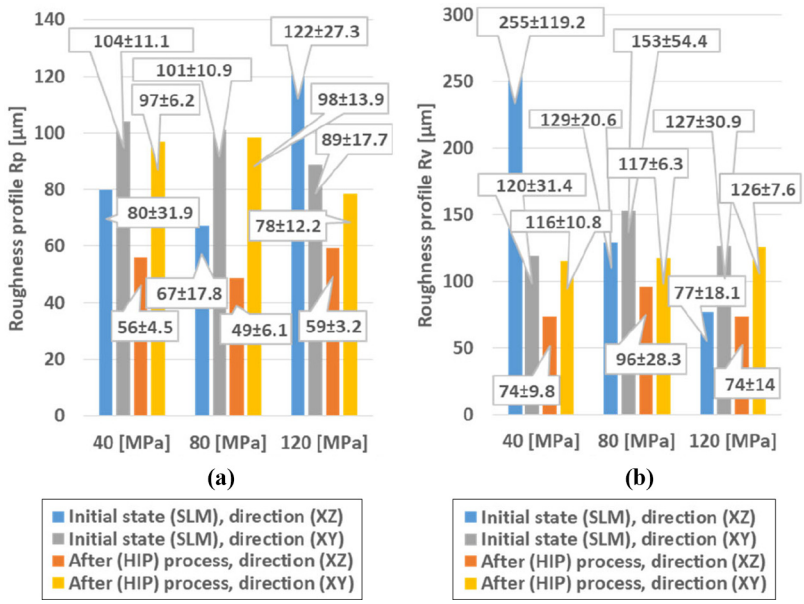

trend can be seen, i.e. the HIP process has caused a decrease in the linear roughness profiles Rp and Rv, see Figure 9. The most significant change was observed for the samples that were carburized for 12 h before the HIP process. The last significant change was then observed for samples that were carburized for 1 h. This is confirmed using both area and local parameters.

Considering the composition of the tested material WC-Co and its thermal properties and the properties of the printed material in the form of inserts. Probably the surface structure was changed due to the action of the near-melting temperature of Co. And due to this there was a merging of protrusions and depressions just evaluated Rvk, Rpk, Rv and Rp parameters. Due to the use of a low power laser and a powder with a lower binder content, which has a significantly lower melting temperature than tungsten carbide particles, a small volume of melt was formed when the laser contacted the powder bed. The capillary forces between the unmelted powder particles were thus not as pronounced, there was no significant shrinkage of the samples, and their surface was thus largely formed by the pores and partly-melted particles of the powder used. The higher surface quality of the samples in the construction direction (XZ direction) is because there is multiple remelting and heating of the applied layers by the subsequent layers. This then leads to a reduction in the porosity of the structure of these surfaces. In terms of improving the surface quality of the formed samples, it would then be necessary to modify the parameters that

Figure 9 Comparison of the recorded change in linear profile roughness parameters Rp and Rv for the samples carbon dopped before HIP treatment at 120 Mpa

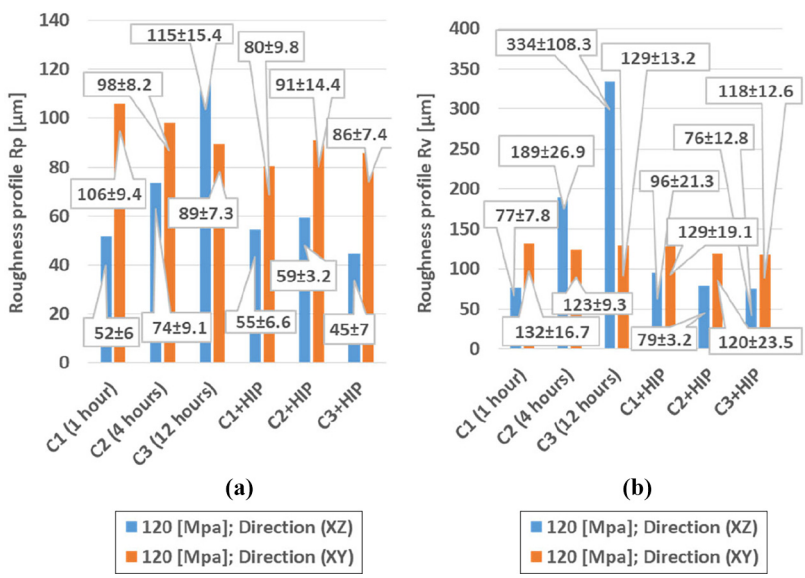

were used to process the samples, for example, to increase the energy input or to use multiple remelting of the powder bed, thus reducing the influence of the balling effect (Zhou *et al.*, 2015a). The microstructures of the samples were analyzed using EDS also. The measurements were aimed at analyzing the chemical composition of the binder Co. In this analysis, the distribution of the dissolved tungsten content was evaluated by EDS using point analysis at the interface between the WC grains and then at the greatest distance from the WC grain boundaries in the Co binder. The approximate measurement areas are shown in Figure 10. The results of EDS analysis are summarized in Table 5. The observed differences in the microstructures of the samples are summarized in Figures 11–12.

The structures of the samples after SLM are heterogeneous. As described above, the structure of the CC contained areas with a higher proportion of binder and coarse tungsten carbide particles and areas with a very fine fraction of tungsten carbides and a low proportion of binder. Sub microscopic tungsten carbide particles are visible in the binder volume, as shown in Figure 11(a). During the subsequent carburizing process, the proportion of these particles in the binder gradually decreased, as shown in Figure 11(b)–11(d). The long-term carburizing process for 12 h resulted in an increase in the porosity of the binder structure [Figure 11(d)]. This was because of its interaction with oxygen in the surrounding environment used to carburize the structure of the samples. The subsequent HIP process resulted in a complete reduction of these fine particles, and the final structure of the samples was composed of coarse tungsten carbide particles and a Co binder, as shown in Figure 12. Table 5 shows the gradual reduction in the proportion of tungsten in the binder. As the proportion of carbon in the binder volume increases, the proportion of tungsten in the binder volume gradually decreases. Therefore, the samples carburized for the longest period had the lowest tungsten content in the Co binder region. The measurement at the WC grain edge was partly influenced by the resolution of the method used to determine the chemical compositions of the samples.

Subsequent sample processing using HIP almost equalizes the tungsten content on the WC/Co interface and in the middle

Figure 10 Identification of the areas where EDS spot analysis was performed

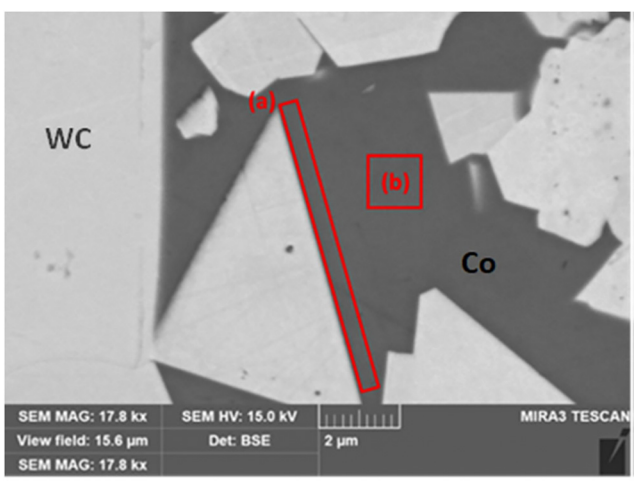

of the Co binder. The proportion of dissolved tungsten in a binder affects its phase composition, mechanical properties, corrosion resistance and thermal stability (Marshall and Giraudel, 2015). Therefore, its volume in the binder and further use of CC are very important. The proportions of tungsten, carbon and binder at the WC grain interface also play a crucial role in the formation of the eta phase, which can precipitate in these areas. Owing to changes in the tungsten content in the binder, carbon doping of the CC microstructure and dissolution of sub microscopic grains, a gradual increase in the size of coarse WC grains occurred during carburizing and HIP. The final size of the WC grains depends on their initial size, temperature and processing time (Sun *et al.*, 2007). One of the main mechanisms of WC grain growth is usually referred to as the Ostwald mechanism (Sun *et al.*, 2007). This involves the dissolution of small grains and their reprecipitation on coarse grains, resulting in the gradual growth and coarsening of large WC grains. This is a spontaneous process driven by the system's attempt to reduce the total energy at the interface between the binder and WC grains. Another mechanism involved is the coalescence of appropriately oriented grains, which results in a reduction in the number of grain boundaries and thus a reduction in energy along the boundaries of the WC grains (Wang *et al.*, 2008). The literature further suggests that higher carbon enrichment of the binder increases the growth rate of the carbide grains (Chabretou *et al.*, 2003), which leads to the assumption that a more pronounced coarsening of the carbide grains occurs during long-term carburization.

X-ray diffraction analysis

In the first phase of this part of the experiment, X-ray diffraction analysis of the phase composition was focused on a group of samples treated by SLM and samples that were then carburized for 1, 4 and 12 h, as shown in Figure 13. In the cutout of image, Figure 13(a), the portion between 38 and 54° [2ϑ] is highlighted, which illustrates the improvement in the readability of the cobalt phase in the samples after carburizing their microstructure. Figure 13(b) shows the diffraction record of the sample under the initial SLM condition. Here, the leading phases are the W_2C phase, which is predominant, and WC phases. The difference between the two phases lies in the lattice parameters and spatial group. Both phases have the same crystal hexagonal lattice, but the W_2C phase has lattice parameters of 2.9970/2.9970/4.7279 [nm] and a space group of 164. In contrast, the WC phase has a space group of 187 and lattice parameters of 2.9060/2.9060/2.8370 [nm]. As shown in Figure 13(c), there was a marked difference between the sample in the initial SLM condition and the samples after carburizing. All sharp diffraction maxima of the cemented samples belong to the WC phase. The Co_4W_2C intermetallic phase is completely absent or below the detection limit of the method used. Subsequently, the changes in crystallite size (coherently diffracting regions) and microstrain within the lattice were analyzed. The use of diffraction planes was chosen for the evaluation to increase the clarity of the images compared to the use of diffraction angles. Figure 14(a) shows the crystallite size distribution for each diffraction plane. From the plot, the crystallite size equalization was visible. The

Table 5 Representation of tungsten in Co binder

		Processing method		
Evaluation area	**SLM**	**SLM + Carburization 1 h**	**SLM + Carburization 4 h**	**SLM + Carburization 12 h**
Interface WC/Co	81 ± 15.5	50 ± 9.7	34 ± 4.1	14 ± 3.6
Co	62 ± 4.9	52 ± 10.0	33 ± 9.3	3 ± 0.4
Evaluation area			Processing method	
	SLM + HIP 40 MPa	SLM + Carburization 1 h + HIP 40 MPa	SLM + Carburization 4 h + HIP 40 MPa	SLM + Carburization 12 h + HIP 40 MPa
Interface WC/Co	32 ± 7.3	22 ± 0.2	7 ± 1.2	10 ± 2.4
Co	26 ± 0.1	26 ± 2.9	6 ± 0.1	6 ± 0.2
HIP 80 MPa				
Evaluation area			Processing method	
	SLM + HIP 80 MPa	SLM + Carburization 1 h + HIP 80 MPa	SLM + Carburization 4 h + HIP 80 MPa	SLM + Carburization 12 h + HIP 80 MPa
Interface WC/Co	42 ± 12.3	23 ± 1	11 ± 3.6	7 ± 0.7
Co	24 ± 0.4	20 ± 0.1	9 ± 0.1	7 ± 0.1
Evaluation area			Processing method	
	SLM + HIP 120 MPa	SLM + Carburization 1 h + HIP 120 MPa	SLM + Carburization 4 h + HIP 120 MPa	SLM + Carburization 12 h + HIP 120 MPa
Interface WC/Co	30 ± 1.2	32 ± 4.9	9 ± 0.9	7 ± 1
Co	24 ± 0.5	23 ± 0.7	9 ± 0.2	6 ± 0.1

Figure 11 (a) Structure of the sample processed by SLM; (b) structure of the sample carburized for 1 h; (c) structure of the sample carburized for 4 h; and (d) structure of the sample carburized for 12 h

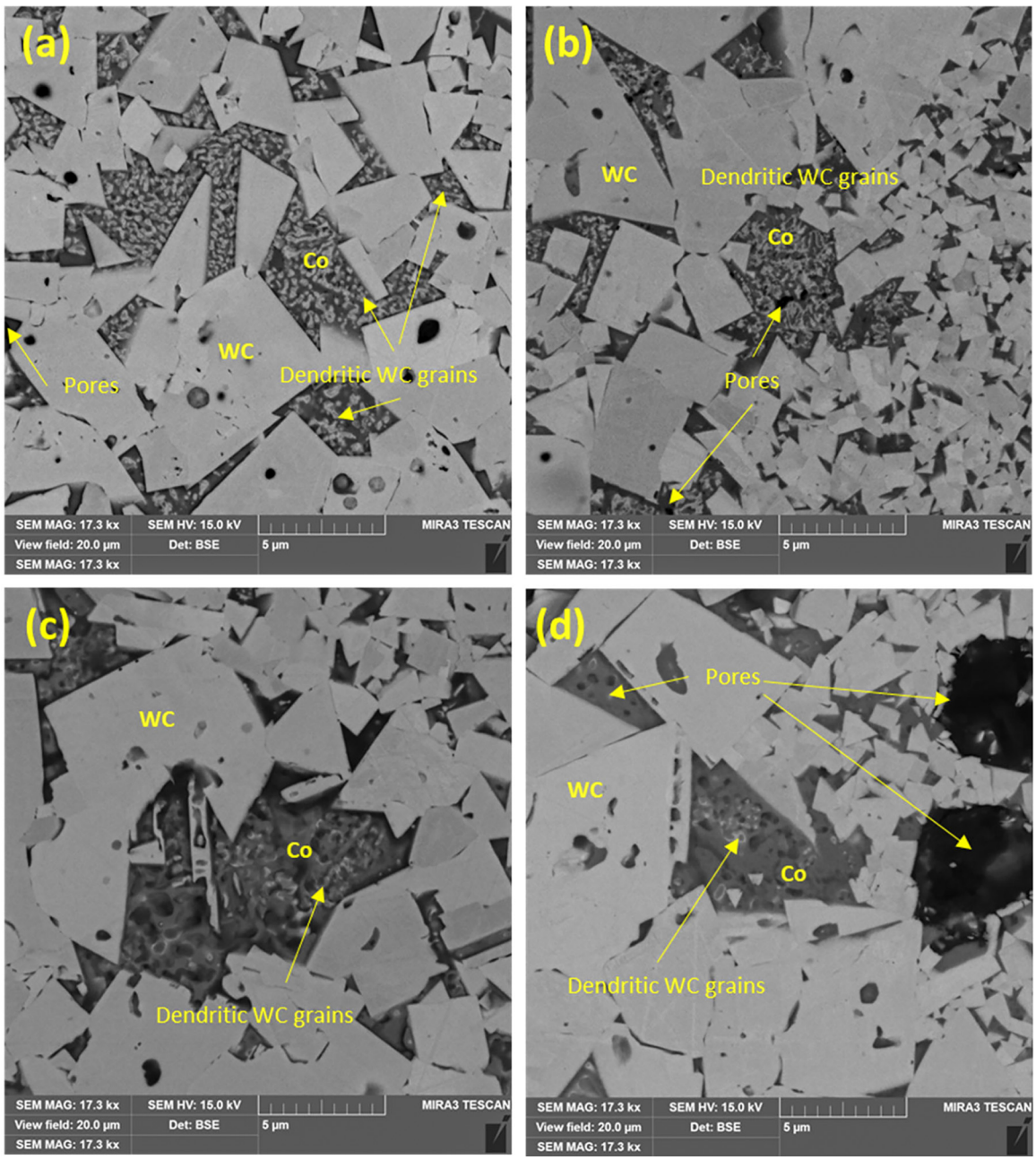

opposite effect is visible in Figure 14(b), in which the waveform of the microstrain size in the lattice is shown. For the Figs, splitting into two plots is used because the samples in the original SLM state represent the state with the W_2C majority phase, compared to the other samples where the WC majority phase is. After the evaluation of the first phase of the experiment, additional samples were measured and divided into three groups. The groups differed in the magnitude of the pressures used in the HIP process, with pressures of 40, 80 and 120 MPa used. Each group of samples consisted of a sample that underwent only the HIP process after the SLM process and samples that underwent carburizing of their microstructure for 1, 4 and 12 h in the intermediate step. Figure 15 shows a comparison of the diffraction records of a series of samples processed by the HIP technology at a pressure of 40 MPa. A graded background comparison was used for analysis. There was an observable difference between the samples that were subjected to complete processing, that is, prior carburizing and HIP processing, and the HIP samples processed only after SLM processing. As in the previous comparison, all sharp diffraction maxima belong to the same phase, namely, the tungsten carbide phase. Figure 15(a) shows the difference between the samples carburized prior to hipping and the hipped-only sample. In

Figure 12 (a) Structure of the sample treated with HIP at 120 MPa; (b) structure of the sample treated with carburizing for 1 h before HIP at 120 MPa; (c) structure of a sample subjected to carburizing treatment for 4 h, before HIP at 120 MPa; and (d) structure of a sample subjected to carburizing treatment for 12 h, before HIP at 120 Mpa

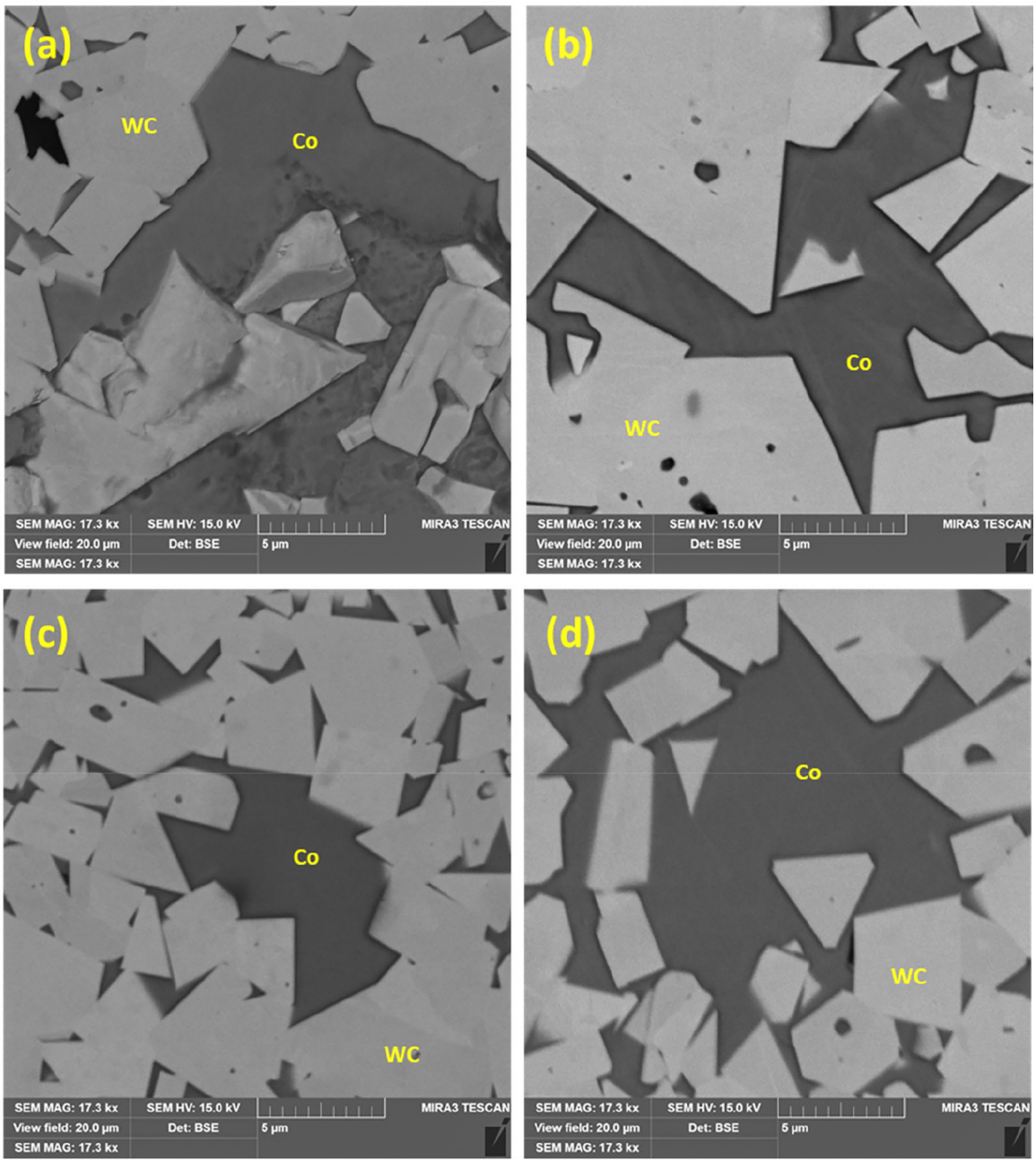

this sample, a minority Co_3W_3C phase was present in the structure, which broke down during carburizing HT and was no longer present in the diffraction patterns of the carburized samples. Only in the sample after 1 h of carburizing, a different intermetallic phase, Co_6W_6C, appeared in the structure, which was not observed in samples with a longer carburizing time. Figure 15(b) shows the crystallite sizes of the samples processed at 40 MPa. Again, the effects of longer processing time and thermal influence on the sample structure can be observed. The sample that was carburized for 12 h showed equalization of the crystallite size and a smoother progression than the other samples. There is a clear difference in the HIP processed sample only, where the difference in crystallite size was the greatest. Figure 15(c) shows the microstrain along the individual diffraction planes. Micro deformations express the degree of stress within the crystallographic lattice. They reflect the magnitude of inhomogeneities and imperfections within the elementary lattice that cause stresses between individual atoms and lattice deflections. The influence of carburizing and subsequent HT and the effect of applied pressure are evident on the micro deformation behavior of the studied samples.

Figure 13 (a) Comparison of diffraction recordings of SLM samples and subsequent cementation after 1, 4 and 12 h of cementation; (b) diffractogram of sample in SLM condition with identified phases marked; and (c) diffractogram of sample after 4 h of cementation with identified phases

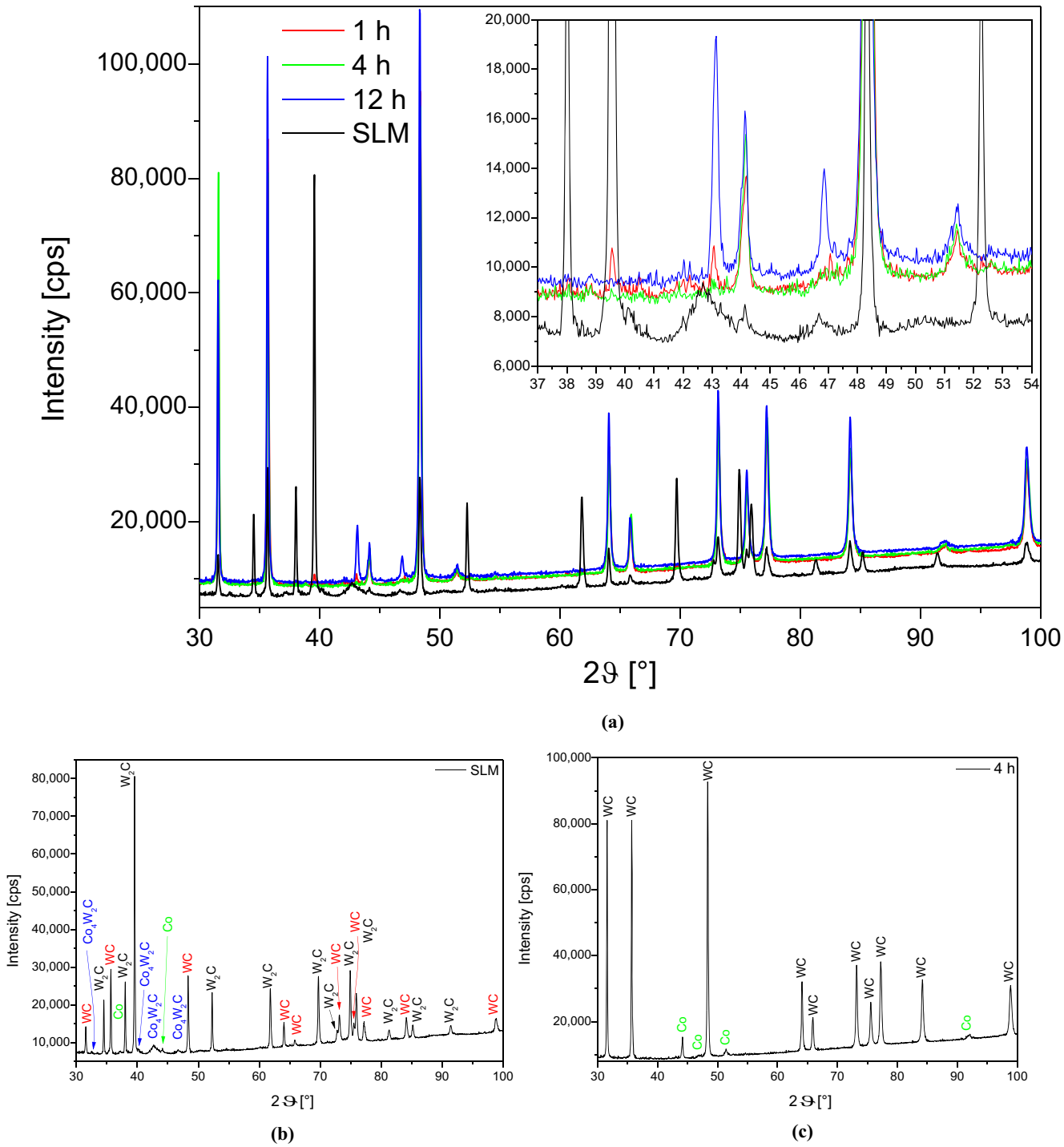

Simultaneously, the distribution of micro deformations depending on the occupation of atoms in the individual planes is evident. The more densely the plane is occupied, or the more interstitial positions are occupied in its vicinity, the higher the micro deformations. With higher temperature and pressure, lattice healing, interstitial rearrangement and reduction of lattice pressure occur. This condition is illustrated by the decreasing value of micro deformations in all the planes studied. When the next two groups of samples were processed, that is, using higher pressures in the HIP process of 80 and 120 MPa, a similar trend was found for the previous series of samples processed at 40 MPa. Invariably, the sample that was only HIP-treated contained diffraction maxima in the structure of the Co_3W_3C phase, which

Figure 14 (a) Comparison of crystallite size in SLM samples and subsequent cementation after 1, 4 and 12 h of cementation; and (b) comparison of micro deformation values in SLM samples and subsequent cementation after 1, 4 and 12 h of cementation

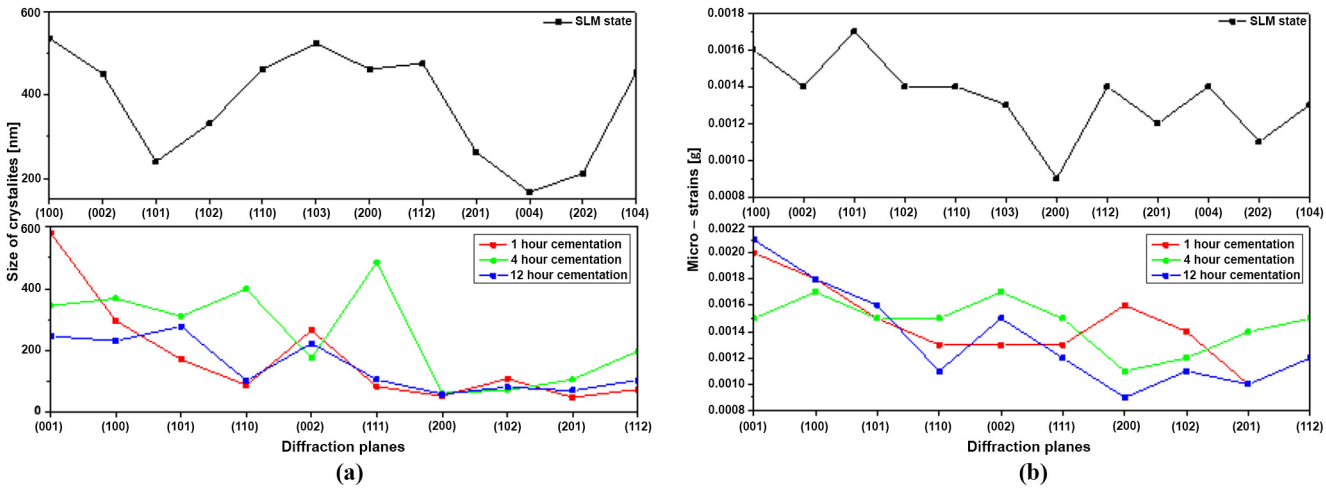

decayed because of the previous processing [see Figures 16(a) and 17(a)]. For both the analyzed series of samples, the sharp diffraction maxima again belong to the major phase WC and the others to Co. Figures 16(b) and 17(b) show the crystallite size distribution for samples processed at 80 MPa and 120 MPa, respectively. The results show that at a pressure of 120 MPa, the alignment in crystallite size was not the same as in the previous cases. The microstrain size distribution in the lattice is shown in Figures 16(c) and 17(c) for the 80 MPa and 120 MPa series samples, respectively. Table 6 summarizes the calculated volume fractions of each structural phase for all batches of samples processed using HIP.

The above results show that additional carbon doping of the CC structure and isostatic hot pressing can increase the homogeneity of their microstructure. In a study (Wei *et al.*, 2012) that deals with the carbon doping of WC-Co powder structure, it is reported that during the sintering process with the coexistence of the liquid phase, a reaction between free carbon and η-phase may occur. This then gradually leads to the formation of the WC and Co phases, so that the final CC structure is made up of only these structural components. At low temperatures, around 900°C, as reported in the study (Shen *et al.*, 2013), the diffusion of carbon is slow, this may lead to insufficient carburization of the CC structure and the conversion of the η-phase to the WC-Co structure does not occur. However, as our experimental results show, at longer carburization times, the gradual decay of this phase occurs. Further reduction of the η-phase may occur because of the applied pressure during isostatic hot pressing. In a study (Lee and Kang, 2006) dealing with the sintering of WC-Co nano powder, it is reported that this phase is reduced when the applied pressure is increased. This is confirmed by the results of our experiment, however, an increase in pressure in the range of 200–400 MPa induces abnormal growth of WC grains. The growth in WC grain size also occurs due to the increase in carbon concentration in the Co binder. In a study (Konyashin *et al.*, 2009), which studies the coarsening of the WC phase in WC-Co sintered carbides with different carbon contents, the results show that the coarsening of WC grains can be reduced by decreasing the carbon concentration and increasing the tungsten concentration in the Co binder. This leads to the conclusion that the opposite phenomenon was occurring in our experiment i.e. the coarsening of the WC grains. Due to the growth of WC grains, the porosity of the CC structure then decreases. As shown in the study of (Mashhadikarimi *et al.*, 2016) and (Zhou *et al.*, 2015b), the relative density of CC structure increases with increasing sintering temperature. At higher sintering temperatures, a higher volume of the liquid phase is formed, which wets and penetrates among the WC grains, thus reducing the porosity of the CC structure. At excessively high sintering temperatures, the WC grains are significantly coarsened, which leads to a deterioration in the mechanical properties of the CC. In addition to the temperature, the applied pressure also affects the compaction of the CC structure. At higher values and constant sintering temperature, the sintering pressure can lead to more pronounced compaction of the WC-Co structure (Petersson and Ågren, 2004) and an increase in its density. Thus, it can be stated that in our experiment, due to increasing pressure, there was a more pronounced coarsening of WC grains and closing of pores in the CC microstructure. This then led to an increase in their density.

Conclusion

The aim of this case study was to assess the effect of carburizing followed by HIP processing on the structure and properties of WC-Co prints made using SLM technology. The results of the experiments show us that the structure of samples is more homogeneous after their processing by the used methods. The main results of our experiment are summarized as follows:

- The measured roughness profiles Rp and Rv varied according to the position of the measured surface relative to the direction of specimen construction. In the XZ direction, the roughness profiles in most cases were lower than those in the XY direction.
- Because of the HIP process, the measured linear roughness profiles Rp and Rv were reduced in both the carburized and non-carburized samples.

Figure 15 (a) Comparison of diffraction recordings for post-HIP (40H1) and pre-HIP samples carburized for 1 h (1CH6), 4 h (4CH6) and 12 h (12CH6); (b) comparison of crystallite size for post-HIP (40H1) and pre-HIP samples carburized for 1 h (1CH6), 4 h (4CH6) and 12 h (12CH6); and (c) comparison of micro deformation values for post-HIP (40H1) and pre-HIP samples carburized for 1 h (1CH6), 4 h (4CH6) and 12 h (12CH6)

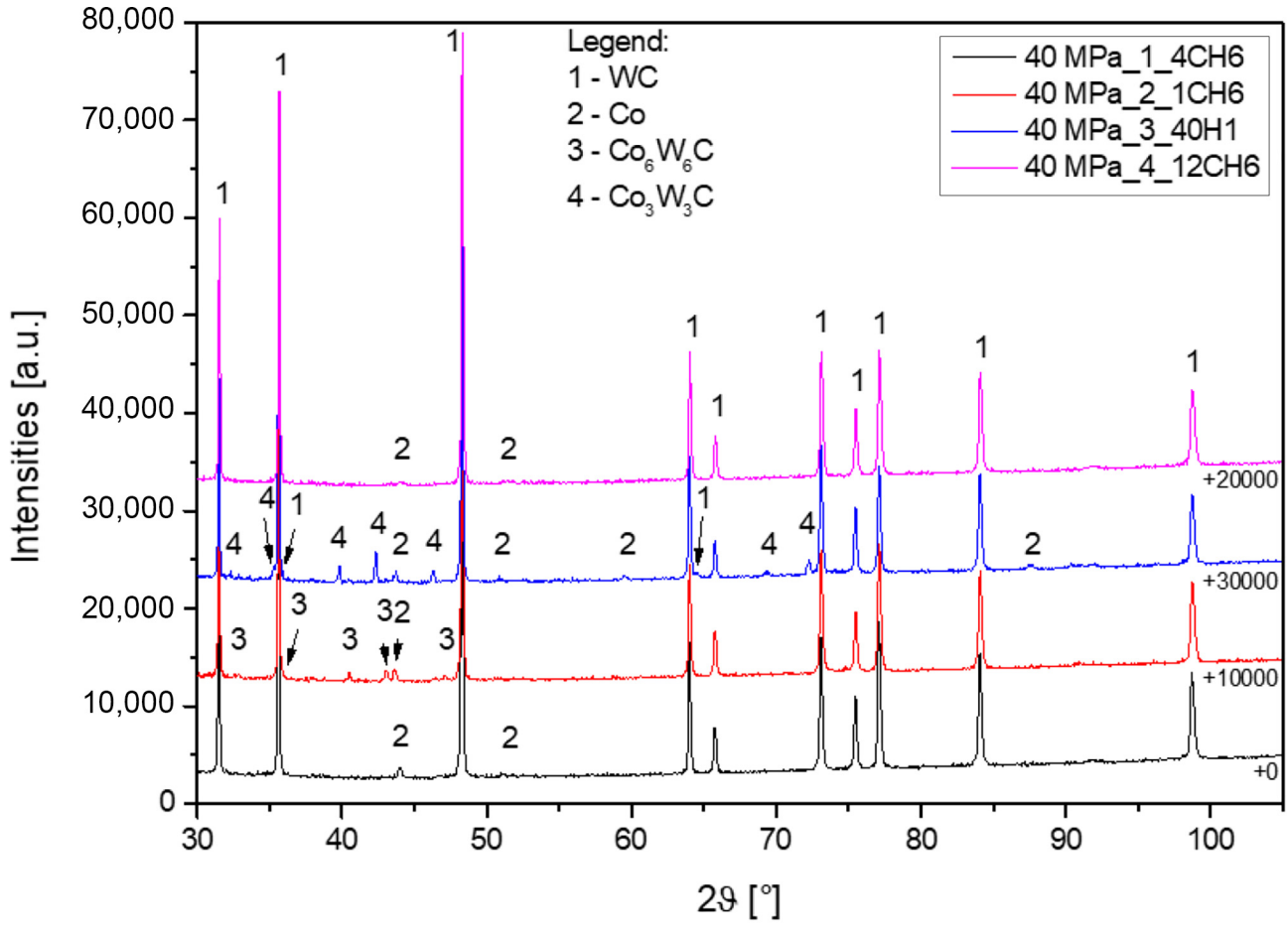

(a)

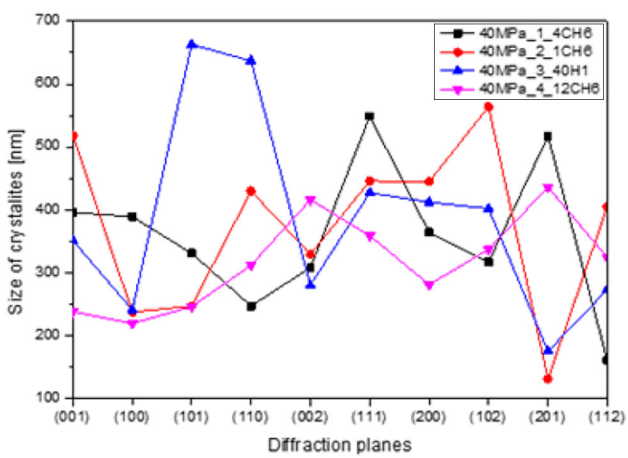

(b)

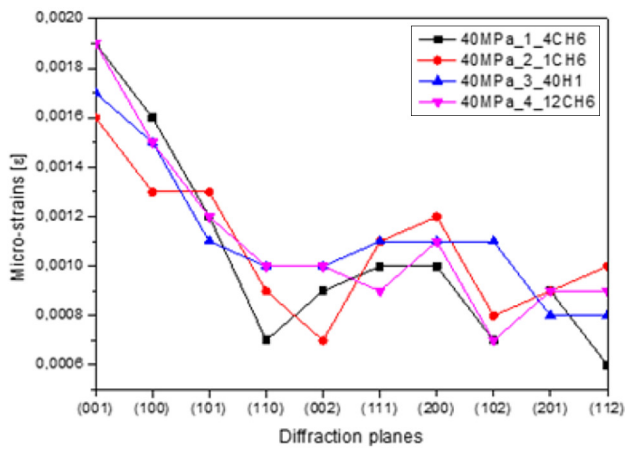

(c)

- Increasing the carburizing time caused a decrease in the proportion of sub microscopic particles in the binder structure and the gradual oxidation of the binder, which led to the formation of pores in its structure.
- Increasing the carburizing time led to a gradual decrease in the proportion of tungsten dissolved in the binder Co. Subsequent sample processing using HIP almost equalizes the tungsten content on the WC/Co interface and in the middle of the Co binder

Figure 16 (a) Comparison of diffraction recordings for post-HIP (80H1) and pre-HIP samples carburized for 1 h (1CH3), 4 h (4CH3) and 12 h (12CH3); (b) comparison of crystallite size for post-HIP (80H1) and pre-HIP samples carburized for 1 h (1CH3), 4 h (4CH3) and 12 h (12CH3); and (c) comparison of micro deformation values for post-HIP (80H1) and pre-HIP samples carburized for 1 h (1CH3), 4 h (4CH3) and 12 h (12CH3)

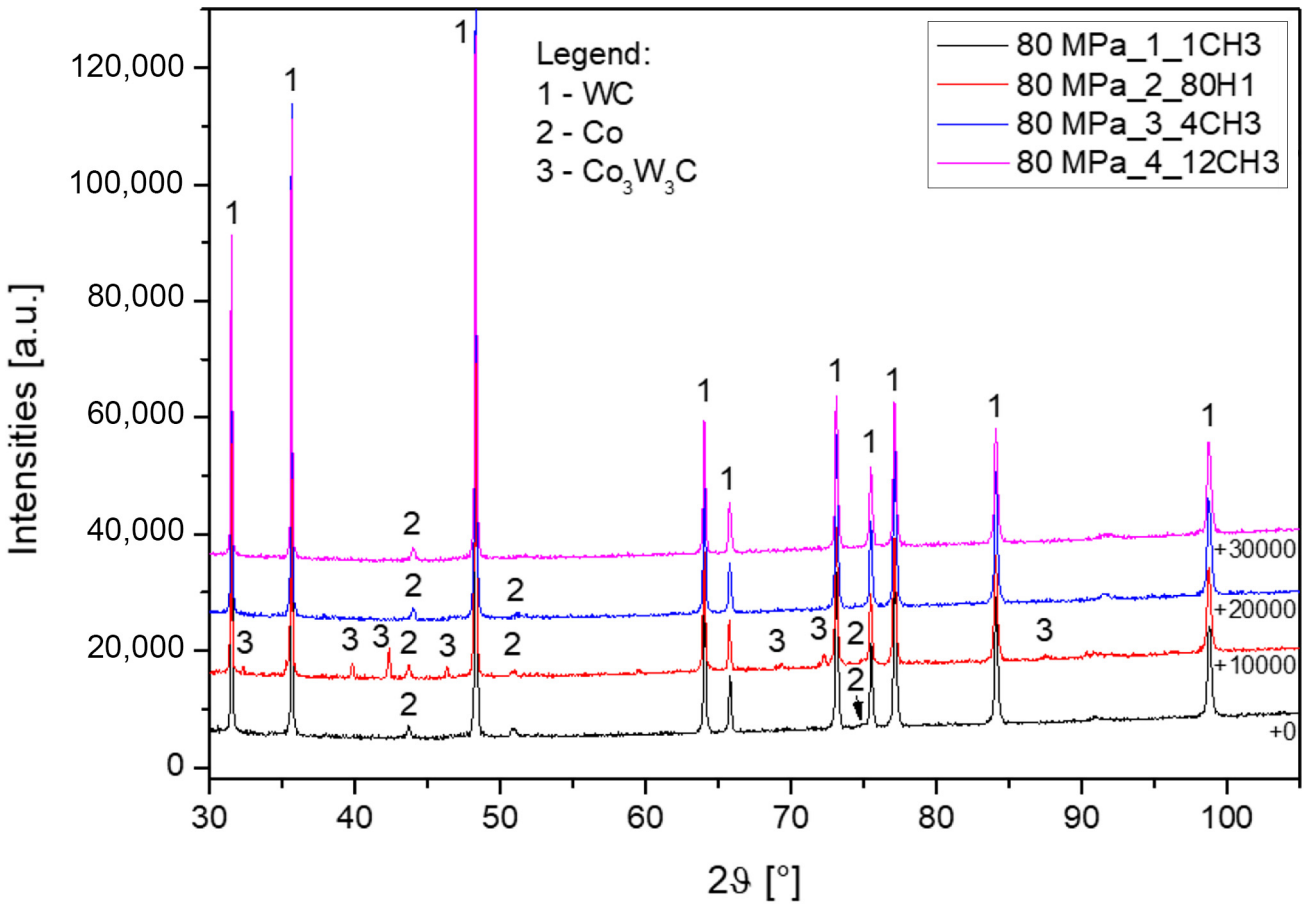

(a)

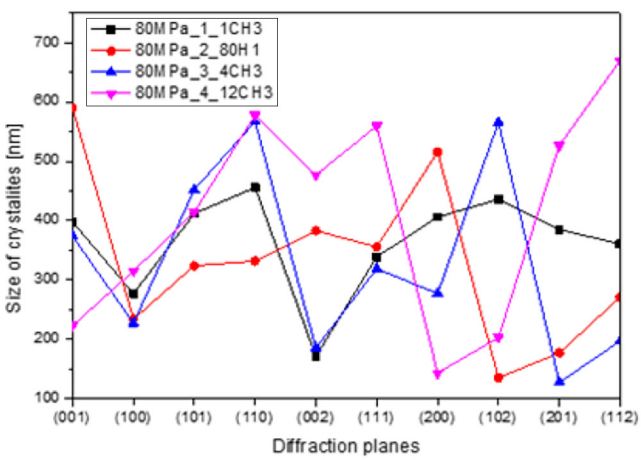

(b)

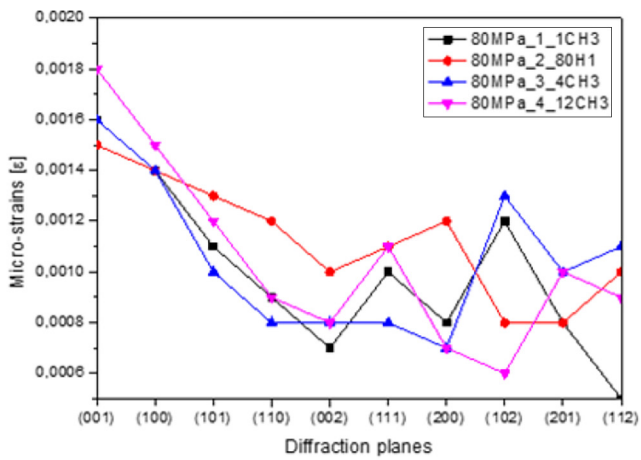

(c)

- Coarsening of the WC phase by various mechanisms was observed during the carburizing and subsequent HIP processes.
- X-ray diffraction analysis of the phase composition showed that during the carburizing and HIP processes, the structural phases W_2C, Co_4W_2C, Co_3W_3C and Co_6W_6C gradually decayed.
- The processing method of the samples further influenced the crystallite size distribution of the major WC phase and microstrain. For samples processed by HIP treatment at a

Table 6 Comparison of phase ratio for differently processed samples

		HIP 40 MPa		
Phase	**HIP**	**HIP + Carburization 1 h**	**HIP + Carburization 4 h**	**HIP + Carburization 12 h**
WC	89.8	95.25	96.04	98
Co	2.79	2.41	3.96	2
Co_6W_6C	0	2.34	0	0
Co_3W_3C	7.41	0	0	0
HIP 80 MPa				
Phase	HIP	HIP + Carburization 1 h	HIP + Carburization 4 h	HIP + Carburization 12 h
WC	90.1	98.35	98.05	98.11
Co	2.53	1.65	1.95	1.89
Co_6W_6C	0	0	0	0
Co_3W_3C	7.37	0	0	0
HIP 120 MPa				
Phase	HIP	HIP + Carburization 1 h	HIP + Carburization 4 h	HIP + Carburization 12 h
WC	83.96	98.44	98.6	98.6
Co	2.07	1.56	1.4	1.4
Co_6W_6C	0	0	0	0
Co_3W_3C	13.97	0	0	0

Figure 17 (a) Comparison of diffraction recordings for post-HIP (120H1) and pre-HIP samples carburized for 1 h (1CH1), 4 h (4CH1) and 12 h (12CH1); (b) comparison of crystallite size for post-HIP (120H1) and pre-HIP samples carburized for 1 h (1CH1), 4 h (4CH1) and 12 h (12CH1); and (c) comparison of micro deformation values for post-HIP (120H1) and pre-HIP samples carburized for 1 h (1CH1), 4 h (4CH1) and 12 h (12CH1)

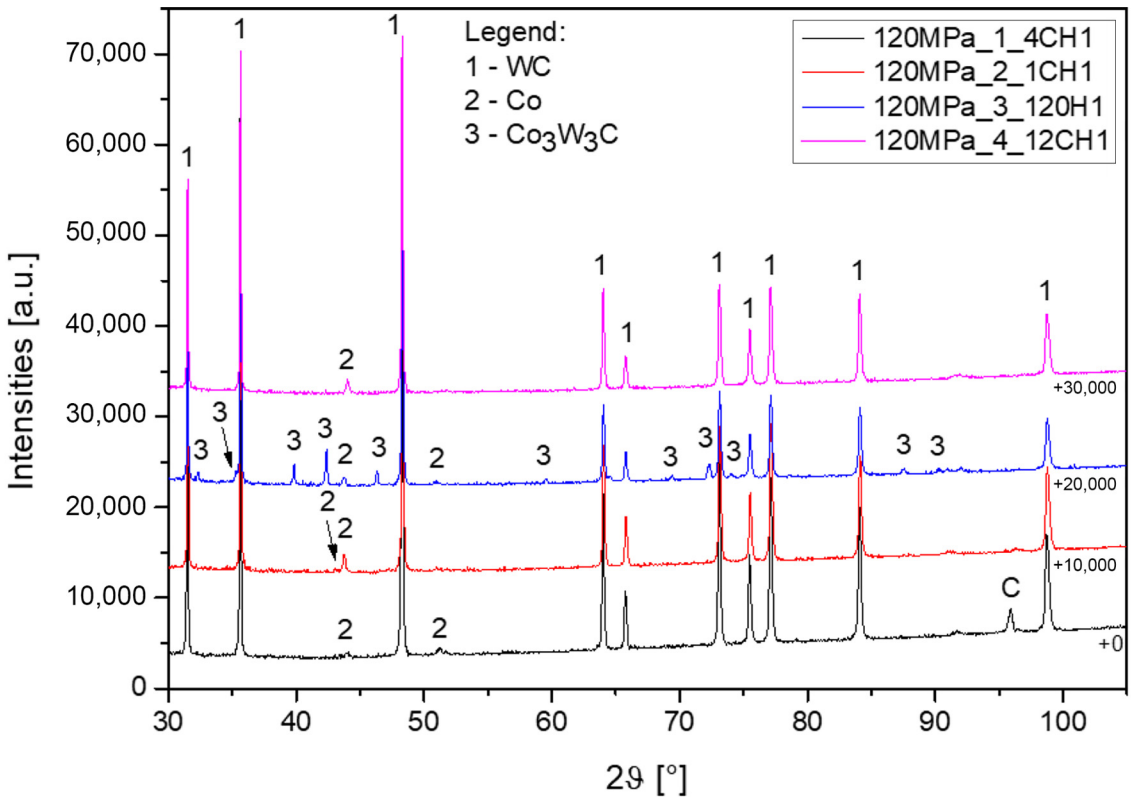

(a)

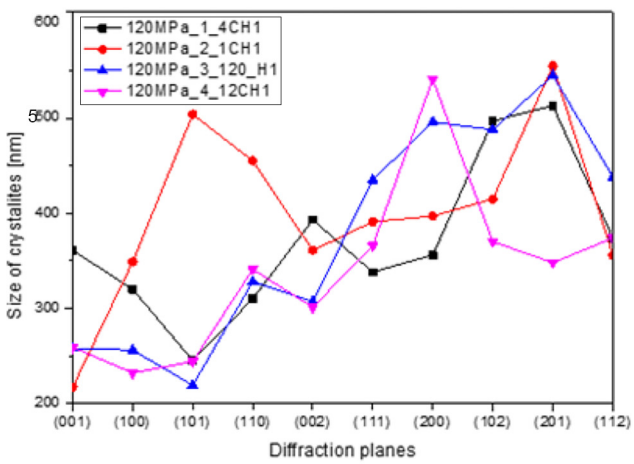

(b)

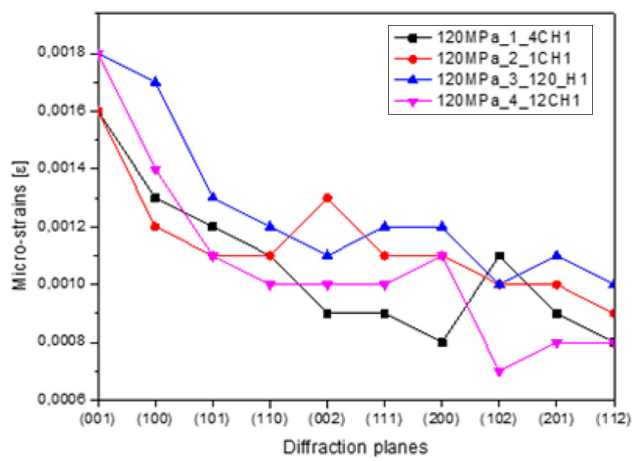

(c)

pressure of 80 MPa or 120 MPa, there was a gradual equilibration in the size of the major WC phase crystallites. The opposite effect was observed for the microstrain.

Further experiments planned after this part of the research will focus on the preparation of particle composite materials for processing using various 3D -printing technologies.

Acknowledgements

This work was conducted within the SUSEN research infrastructure established in the framework of the European Regional Development Fund (ERDF) in project CZ.1.05/2.1.00/03.0108 and the European Structural and Investment Funds (ESIF) in project CZ.02.1.01/0.0/0.0/15_008/0000293.

This work was also supported by the SGS-2021–030 project "Development of new materials, application of modern methods of their processing, ecological production, welding and testing." The paper was also supported by the Technology Agency of the Czech Republic as part of the ZETA program (no. TJ01000218, "Manufacture of carbide cutting tool prototype using SLM additive manufacturing technology." This result was produced by the CEDAMNF project Reg. no. CZ.02.1.01/0.0/0.0/15_003/0000358, which is co-financed by the ERDF under the Ministry of Education and Science's OP VVV program.

Ethical compliance: All procedures performed in studies involving human participants were in accordance with the ethical standards of the institutional and/or national research committee and with the 1964 Helsinki Declaration and its later amendments or comparable ethical standards.

References

ASM International (1992), "Volume 3- alloy phase diagrams", pp. 523-524, ISBN: 0-87170-381-5.

ASTM (2000), *ASTM B657-18 Standard Guide for Metallographic Identification of Microstructure in Cemented Carbides*, ASTM International, West Conshohocken, PA.

Bai, S., Perevoshchikova, N., Sha, Y. and Wu, X. (2019), "The effects of selective laser melting process parameters on relative density of the AlSi10Mg parts and suitable procedures of the Archimedes method", *Applied Sciences*, Vol. 9 No. 3, p. 583, doi: 10.3390/app9030583.

Bricín, D., Ackermann, M., Jansa, Z., Kubátová, D., Kříž, A., Špirit, Z. and Šafka, J. (2020), "Development of the structure of cemented carbides during their processing by SLM and HIP", *Metals*, Vol. 10 No. 11, p. 1477, doi: 10.3390/met10111477.

Bricín, D., Elmanova, A. and Kříž, K. (2019), "The effect of selective laser melting technology on the development of the structure of samples made from WC-Co powder", *Journal of International Scientific Publications: Materials, Methods & Technologies*, Vol. 13, pp. 38-47, ISSN 1314-7269.

Brookes, K. (2019), "EPMA considers additive manufacturing for hard metals", *Metal Powder Report*, Vol. 74 No. 3, pp. 141-157, doi: 10.1016/j.mprp.2019.04.057.

Budin, S., Ria Jaafar, T. and Asri Selamat, M. (2017), "Effect of sintering atmosphere on the mechanical properties of sintered tungsten carbide", *MATEC Web of Conferences*, Vol. 130, p. 3006, doi: 10.1051/matecconf/201713003006.

Campanelli, S., Contuzzi, N., Posa, P. and Angelastro, A. (2019), "Printability and microstructure of selective laser melting of WC/Co/Cr powder", *Materials*, Vol. 12 No. 15, p. 2397, doi: 10.3390/ma12152397.

Chabretou, V., Allibert, C. and Missiaen, J. (2003), "Quantitative analysis of the effect of the binder phase composition on grain growth in WC-Co sintered materials", *Journal of Materials Science*, Vol. 38 No. 12, pp. 2581-2590, doi: 10.1023/A:1024418131674.

Chen, J., Huang, M., Fang, Z., Koopman, M., Liu, W., Deng, X., Zhao, Z., Chen, S., Wu, S., Liu, J., Qi, W. and Wang, Z. (2019), "Microstructure analysis of high density WC-Co composite prepared by one step selective laser melting", *International Journal of Refractory Metals and Hard Materials*, Vol. 84, p. 104980, doi: 10.1016/j.ijrmhm.2019.104980.

Domashenkov, A., Borbély, A. and Smurov, I. (2016), "Structural modifications of WC/Co nanophased and conventional powders processed by selective laser melting", *Materials and Manufacturing Processes*, Vol. 32 No. 1, pp. 93-100, doi: 10.1080/10426914.2016.1176195.

Eso, O., Fang, Z. and Griffo, A. (2007), "Kinetics of cobalt gradient formation during the liquid phase sintering of functionally graded WC–Co", *International Journal of Refractory Metals and Hard Materials*, Vol. 25 No. 4, pp. 286-292, doi: 10.1016/j.ijrmhm.2006.07.002.

Formisano, A., Capece Minutolo, F., Caraviello, A., Carrino, L., Durante, M. and Langella, A. (2016), "Influence of Eta-Phase on wear behavior of WC-Co carbides", *Advances in Tribology*, Vol. 2016, pp. 1-6, doi: 10.1155/2016/5063274.

Fortunato, A., Valli, G., Liverani, E. and Ascari, A. (2019), "Additive manufacturing of WC-Co cutting tools for gear production", *Lasers in Manufacturing and Materials Processing*, Vol. 6 No. 3, pp. 247-262, doi: 10.1007/s40516-019-00092-0.

Fries, S., Genilke, S., Wilms, M., Seimann, M., Weisheit, A., Kaletsch, A., Bergs, T., Schleifenbaum, J. and Broeckmann, C. (2020), "Laser-based additive manufacturing of WC–Co with high-temperature powder bed preheating", †. *Steel Research International*, Vol. 91 No. 3, p. 1900511, doi: 10.1002/srin.201900511.

García, J., Collado Ciprés, V., Blomqvist, A. and Kaplan, B. (2019), "Cemented carbide microstructures: a review", *International Journal of Refractory Metals and Hard Materials*, Vol. 80, pp. 40-68, doi: 10.1016/j.ijrmhm.2018.12.004.

GTP (2022), "Globaltungsten.com.2022.[online]", available at: www.globaltungsten.com/fileadmin/user_upload/AM-Grade WC701.pdf (accessed 2 August 2022).

Gu, D. and Meiners, W. (2010), "Microstructure characteristics and formation mechanisms of in situ WC cemented carbide based hard metals prepared by selective laser melting", *Materials Science and Engineering: A*, Vol. 527 Nos 29/30, pp. 7585-7592, doi: 10.1016/j.msea.2010.08.075.

Gusarov, A., Pavlov, M. and Smurov, I. (2011), "Residual stresses at laser surface remelting and additive manufacturing", *Physics Procedia*, Vol. 12, pp. 248-254, doi: 10.1016/j.phpro.2011.03.032.

Ishida, K. and Nishizawa, T. (1991), "The C-Co(carbon-cobalt) system", *Journal of Phase Equilibria*, Vol. 12 No. 4, pp. 417-424, doi: 10.1007/BF02645959.

Khmyrov, R., Safronov, V. and Gusarov, A. (2016), "Obtaining crack-free WC-Co alloys by selective laser melting", *Physics Procedia*, Vol. 83, pp. 874-881, doi: 10.1016/j.phpro.2016.08.091.

Konyashin, I., Hlawatschek, S., Ries, B., Lachmann, F., Dorn, F., Sologubenko, A. and Weirich, T. (2009), "On the mechanism of WC coarsening in WC–Co hard metals with various carbon contents", *International Journal of Refractory Metals and Hard Materials*, Vol. 27 No. 2, pp. 234-243, doi: 10.1016/j.ijrmhm.2008.09.001.

Ku, N., Pittari, J., Kilczewski, S. and Kudzal, A. (2019), "Additive manufacturing of cemented tungsten carbide with a cobalt-free alloy binder by selective laser melting for high-hardness applications", *JOM*, Vol. 71 No. 4, pp. 1535-1542, doi: 10.1007/s11837-019-03366-2.

Kubatova, D. and Melichar, M. (2019), "Roughness evaluation using Abbott-Firestone curve parameters", *Proceedings of the*

30th DAAAM International Symposium, in Katalinic, V. (Ed.), DAAAM International, Vienna, pp. 467-475, ISBN 978-3-902734-22-8, ISSN 1726-9679, doi: 10.2507/30th.daaam.proceedings.063

Kublii, V. and Velikanova, T. (2004), "Ordering in the carbide W2C and phase equilibria in the tungsten? carbon system in the region of its existence", *Powder Metallurgy and Metal Ceramics*, Vol. 43 Nos 11/12, pp. 630-644, doi: 10.1007/s11106-005-0032-3.

Kučerová, L., Burdová, K., Jeníček, Š. and Chena, I. (2021), "Effect of solution annealing and precipitation hardening at 250°C–550°C on microstructure and mechanical properties of additively manufactured 1.2709 maraging steel", *Materials Science and Engineering: A*, Vol. 814, p. 141195, doi: 10.1016/j.msea.2021.141195.

Kumar, S. (2009), "Manufacturing of WC–Co moulds using SLS machine", *Journal of Materials Processing Technology*, Vol. 209 No. 8, pp. 3840-3848, doi: 10.1016/j.jmatprotec.2008.08.037.

Kumar, S. (2018), "Process chain development for additive manufacturing of cemented carbide", *Journal of Manufacturing Processes*, Vol. 34, pp. 121-130, doi: 10.1016/j.jmapro.2018.05.036.

Lassner, E. and Schubert, W. (2012), *Tungsten: Properties, Chemistry, Technology of the Element, Alloys, and Chemical Compounds*, Springer Science & Business Media, Berlin, pp. 115-123, ISBN 1461549078.

Lee, G. and Kang, S. (2006), "Sintering of nano-sized WC–Co powders produced by a gas reduction–carburization process", *Journal of Alloys and Compounds*, Vol. 419 Nos 1/2, pp. 281-289, doi: 10.1016/j.jallcom.2005.09.060.

Lu, K. and Lu, J. (2004), "Nanostructured surface layer on metallic materials induced by surface mechanical attrition treatment", *Materials Science and Engineering: A*, Vols 375/377, pp. 38-45, doi: 10.1016/j.msea.2003.10.261.

M, P. (2020), "Additive manufacturing of tungsten carbide hard metal parts by selective laser melting (SLM), selective laser sintering (SLS) and binder jet 3D printing (BJ3DP) techniques", *Lasers in Manufacturing and Materials Processing*, Vol. 7 No. 3, pp. 338-371, doi: 10.1007/s40516-020-00124-0.

Marshall, J. and Giraudel, M. (2015), "The role of tungsten in the Co binder: effects on WC grain size and hcp–fcc Co in the binder phase", *International Journal of Refractory Metals and Hard Materials*, Vol. 49, pp. 57-66, doi: 10.1016/j.ijrmhm.2014.09.028.

Mashhadikarimi, M., Gomes, U., Oliveira, M., Guimarães, R. and Filgueira, M. (2016), "Study HTHP sintered WC/Co hard metal", *Materials Research*, Vol. 20 No. 1, pp. 138-143, doi: 10.1590/1980-5373-MR-2016-0471.

Morton, C., Wills, D. and Stjernberg, K. (2005), "The temperature ranges for maximum effectiveness of grain growth inhibitors in WC–Co alloys", *International Journal of Refractory Metals and Hard Materials*, Vol. 23 Nos 4/6, pp. 287-293, doi: 10.1016/j.ijrmhm.2005.05.011.

Nicoletto, G., Maisano, S., Antolotti, M. and Dall'Aglio, F. (2017), "Influence of post fabrication heat treatments on the fatigue behavior of Ti-6Al-4V produced by selective laser melting", *Procedia Structural Integrity*, Vol. 7, pp. 133-140, doi: 10.1016/j.prostr.2017.11.070.

Petersson, A. and Ågren, J. (2004), "Constitutive behaviour of WC–Co materials with different grain size sintered under load", *Acta Materialia*, Vol. 52 No. 7, pp. 1847-1858, doi: 10.1016/j.actamat.2003.12.024.

Pollock, C.B. and Stadelmaier, H.H. (1970), "The eta carbides in the Fe–W–C and Co–W–C systems", *Metall Mater Trans B*, Vol. 1 No. 4, pp. 767-770, doi: 10.1007/BF02811752.

Ponomarev, S., Shatov, A., Mikhailov, A. and Firstov, S. (2015), "Mechanisms for the degradation of strength and wear-resistance of WC based cemented carbides due to faster cooling", *International Journal of Refractory Metals and Hard Materials*, Vol. 49, pp. 161-169, doi: 10.1016/j.ijrmhm.2014.10.010.

Portella, Q., Chemkhi, M. and Retraint, D. (2020), "Influence of surface mechanical attrition treatment (SMAT) post-treatment on microstructural, mechanical and tensile behaviour of additive manufactured AISI 316L", *Materials Characterization*, Vol. 167, p. 110463, doi: 10.1016/j.matchar.2020.110463.

Ptáček, L. (2003), "Nauka o materiálu I. 2., opr. a rozš. vyd. brno: akademické nakladatelství CERM", ISBN 80-7204-283-1.

Sames, W., List, F., Pannala, S., Dehoff, R. and Babu, S. (2016), "The metallurgy and processing science of metal additive manufacturing", *International Materials Reviews*, Vol. 61 No. 5, pp. 315-360, doi: 10.1080/09506608.2015.1116649.

Sarin, V. (2014), *Comprehensive Hard Materials, Volume 1*, Elsevier, Newnes, ISBN: 978-0-444-63385-9.

Shen, T., Xiao, D., Ou, X., Song, M., Li, X. and He, Y. (2013), "Preparation of ultrafine WC-10Co composite powders by reduction and carbonization", *Journal of Central South University*, Vol. 20 No. 8, pp. 2090-2095, doi: 10.1007/s11771-013-1711-8.

Stankevič, V., Čermák, A., Mikalauskas, S., Kožmín, P., Indrišiūnas, S. and Račiukaitis, G. (2018), "Processing of ultra-hard materials with picosecond pulses: from research work to industrial applications", *Journal of Laser Applications*, Vol. 30 No. 3, doi: 10.2351/1.5040633.

Stewart, D., Shipway, P. and McCartney, D. (1998), "Influence of heat treatment on the abrasive wear behaviour of HVOF sprayed WC–Co coatings", *Surface and Coatings Technology*, Vol. 105 No. 1-2, pp. 13-24, doi: 10.1016/S0257-8972(98)00444-7.

Sun, L., Jia, C. and Xian, M. (2007), "A research on the grain growth of WC–Co cemented carbide", *International Journal of Refractory Metals and Hard Materials*, Vol. 25 No. 2, pp. 121-124, doi: 10.1016/j.ijrmhm.2006.03.002.

Sun, L., Yang, T., Jia, C. and Xiong, J. (2011), "Effects of graphite on the microstructure and properties of ultrafine WC-11Co composites by spark plasma sintering", *Rare Metals*, Vol. 30 No. 1, pp. 63-67, doi: 10.1007/s12598-011-0198-4.

Uhlmann, E., Bergmann, A. and Gridin, W. (2015), "Investigation on additive manufacturing of tungsten carbide-cobalt by selective laser melting", *Procedia CIRP*, Vol. 35, pp. 8-15, doi: 10.1016/j.procir.2015.08.060.

Upadhyaya, G. (1998), *Cemented Tungsten Carbides*, William Andrew Publishing, Norwich, New York, NY, ISBN: 0-8155-1417-4.

Vreeswijk, M., Kot, A., Giuliani, F. and Humphry-Baker, S. (2021), "Abnormal WC crystal growth from liquid Co flux occurs via eta phase decomposition", *International Journal of Refractory Metals and Hard Materials*, Vol. 99, p. 105589, doi: 10.1016/j.ijrmhm.2021.105589.

Wang, X., Fang, Z. and Sohn, H. (2008), "Grain growth during the early stage of sintering of nanosized WC–Co powder", *International Journal of Refractory Metals and Hard Materials*, Vol. 26 No. 3, pp. 232-241, doi: 10.1016/j.ijrmhm.2007.04.006.

Wei, C., Song, X., Fu, J., Lv, X., Wang, H., Gao, Y., Zhao, S. and Liu, X. (2012), "Effect of carbon addition on microstructure and properties of WC–Co cemented carbides", *Journal of Materials Science & Technology*, Vol. 28 No. 9, pp. 837-843, doi: 10.1016/S1005-0302(12)60140-6.

Yang, Y., Zhang, C., Wang, D., Nie, L., Wellmann, D. and Tian, Y. (2020), "Additive manufacturing of WC-Co hard metals: a review", *The International Journal of Advanced Manufacturing Technology*, Vol. 108 No. 5-6, pp. 1653-1673, doi: 10.1007/s00170-020-05389-5.

Zhou, X., Liu, X., Zhang, D., Shen, Z. and Liu, W. (2015a), "Balling phenomena in selective laser melted tungsten", *Journal of Materials Processing Technology*, Vol. 222, pp. 33-42, doi: 10.1016/j.jmatprotec.2015.02.032.

Zhou, Y., Yang, Y., Yang, G., Yin, D., Qin, Y. and Liu, J. (2015b), "Effects of sintering temperature on the densification of WC-6Co cemented carbides sintered by coupled multi-physical-fields activated technology", *Manufacturing Review*, Vol. 2, p. 18, doi: 10.1051/mfreview/2015017.

Corresponding author

David Bricín can be contacted at: bricda@kmm.zcu.cz